Available online at www.sciencedirect.com

SCIENCE DIRECT®

Remote Sensing of Environment 95 (2005) 1–13

Remote Sensing of Environment

www.elsevier.com/locate/rse

Review

# Oil spill detection by satellite remote sensing

Camilla Brekke[a,b,*], Anne H.S. Solberg[b]

[a]Norwegian Defence Research Establishment, Postboks 25, 2027 Kjeller, Norway
[b]Department of Informatics, University of Oslo, Postboks 1080 Blindern, 0316 Oslo, Norway

Received 3 September 2004; received in revised form 11 November 2004; accepted 17 November 2004

**Abstract**

This paper presents the state of the art for oil spill detection in the world oceans. We discuss different satellite sensors and oil spill detectability under varying conditions. In particular, we concentrate on the use of manual and automatic approaches to discriminate between oil slicks and look-alikes based on pattern recognition. We conclude with a discussion of suggestions for further research with respect to oil spill detection systems.


*Keywords:* Synthetic aperture radar; Oil spill; Detectability; Manual detection; Automatic algorithms; Dark spot detection; Feature extraction; Classification

**Contents**



## 1. Introduction

Oil spills on the sea surface are seen relatively often. Observed oil spills correlate very well with the major shipping routes (e.g. in the Southeast Asian Waters (Lu,

* Corresponding author. Norwegian Defence Research Establishment, Postboks 25, 2027 Kjeller, Norway. Tel.: +47 63 80 72 31; fax: +47 63 80 72 12.
*E-mail address:* Camilla.Brekke@ffi.no (C. Brekke).

0034-4257/$ - see front matter © 2004 Elsevier Inc. All rights reserved.
doi:10.1016/j.rse.2004.11.015

2003; Lu et al., 1999), and in the Yellow and East China Sea (Ivanov et al., 2002) and commonly appear in connection with offshore installations (e.g. in the North Sea (Espedal & Johannessen, 2000). Annually, 48% of the oil pollution in the oceans are fuels and 29% are crude oil. Tanker accidents contribute with only 5% of all pollution entering into the sea (Fingas, 2001). After analysing 190 ERS-1[1] SAR images of the Mediterranean Sea, Pavlakis et al. (1996) found that "deliberate" oil spills appear with considerably higher frequency than oil spills corresponding to reported ship accidents. According to the European Space Agency (1998), 45% of the oil pollution comes from operative discharges from ships. When taking into account how frequent such spillages occur, controlled regular oil spills can be a much greater threat to the marine environment and the ecosystem than larger oil spill accidents like the Prestige tanker (carrying >77,000 ton of fuel oil (Oceanides Web-site, 2004) accident at Galice, northwest coast of Spain in 2002. The impact of not monitoring oil spills is presently unknown, but the main environmental impact is assumed to be seabirds mistakenly landing on them and the damage to the coastal ecology as spills hit the beach (Shepherd, 2004). Simecek-Beatty and Clemente-Colón (2004) describes how oiled birds lead to the use of SAR for locating a sunken vessel leaking oil.

Active microwave sensors like Synthetic Aperture Radar (SAR) capture two-dimensional images. The image brightness is a reflection of the microwave backscattering properties of the surface. SAR deployed on satellites is today an important tool in oil spill monitoring due to its wide area coverage and day and night all-weather capabilities.

Satellite-based oil pollution monitoring capabilities in the Norwegian waters were demonstrated in the early 1990s by using images from the ERS-1 satellite (e.g. Bern et al., 1992b; Skøelv & Wahl, 1993; Wahl et al., 1994b). A demonstrator system based on ERS for the Spanish coast was presented by Martinez and Moreno (1996). Today, RADARSAT-1 and ENVISAT are the two main providers of satellite SAR images for oil spill monitoring.

Access to an increased amount of SAR images means a growing workload on the operators at analysis centres. In addition, recent research shows that even if the operators go through extensive training to learn manual oil spill detection they can detect different slicks and give them different confidence levels (Indregard et al., 2004). Algorithms for automatic detection that can help in screening the images and prioritising the alarms will be of great benefit. Research on this field has been ongoing for more than a decade, and this paper reviews various methods for satellite-based oil spill detection in the marine environment.

As SAR is just one of many remote sensing sensors available an evaluation of the applicability of other satellite sensors for oil spill monitoring is included as well. Most studies done on airborne remote sensing techniques are excluded. For a review of airborne sensor technology for oil spill observation see Goodman (1994). The detectability of oil spills in SAR images are discussed, in terms of wind conditions, sensor characteristics and ambiguities caused by other phenomena than oil spills. Finally, our emphasis is on methodology and algorithms for oil spill detection in spaceborne SAR imagery.

## 2. Satellite sensors for oil spill detection

Microwaves are commonly used for ocean pollution monitoring by remote sensing. They are often preferred to optical sensors due to the all-weather and all-day capabilities, and examples of SAR-equipped satellites are presented in Table 1. Mainly spaceborne instruments are covered here, but airborne Side-Looking Airborne Radar (SLAR) is another possibility. SLAR is an older but less expensive technology than SAR, but SAR has greater range and resolution (Fingas & Brown, 1997). Airborne surveillance is limited by the high costs and is less efficient for wide area surveillance due to its limited coverage. While spaceborne SAR can be used for a first warning, aircrafts are more suitable to be brought into action to identify the polluter, the extent, and the type of spill. An example is the German aerial surveillance, which locates oil discharges by SLAR, infrared/ultraviolet (IR/UV) scanning is used to quantify the extent of the film, a microwave radiometer (MWR) is used to quantify the thickness and a laser-fluoro-sensor (LFS) is used for oil type classification (Trieschmann et al., 2003).

In addition to SAR, there are other spaceborne remote sensing devices that have some potential for oil spill monitoring. Friedman et al. (2002) compare a RADARSAT-1 SAR image with a corresponding Sea-viewing Wide Field-of-view Sensor (SeaWiFS, visible sensor) image. SeaWiFS measures high levels of chlorophyll for areas with algal bloom, while the SAR images have low backscatter levels in these regions. It is concluded that multiple data sets can be used to discriminate between, for example,

Table 1
Some satellites carrying SAR instruments

| Satellite (sensor) | Operative | Owner | Characteristics |
|---|---|---|---|
| SEASAT | 1978–off same year | NASA | L-band, HH-pol |
| ALMAZ-1 | 1991–1992 | Russian Space Agency | S-band, HH-pol |
| ERS-1 | 1991–1996 | ESA | C-band, VV-pol |
| ERS-2 | 1995–operating | ESA | C-band, VV-pol |
| RADARSAT-1 | 1995–operating | CSA | C band, HH pol |
| ENVISAT (ASAR) | 2002–operating | ESA | C-band, HH and VV, alt. pol., and crosspol. modes |

C-band 4–8 GHz, $\lambda$ 3.75–7.5 cm, L-band 1–2 GHz, $\lambda$ 15–30 cm and S-band 2–4 GHz, $\lambda$ 7.5–15 cm.

[1] ERS-1: the First European Remote Sensing Satellite.

algal blooms and man-made slicks. Indregard et al. (2004) point out that additional information (in addition to SAR) about algal bloom is desirable, particularly in the Baltic Sea. This could be taken from optical imagery, from alga maps or other related information. Fig. 1 shows two examples of algal bloom imaged by SAR.

A drawback of the SeaWiFS sensor is its coarse spatial resolution of ~1 km. Hu et al. (2003) demonstrate the possibility of oil spill monitoring by the Moderate-Resolution Imaging Spectroradiometer (MODIS) instrument, carried onboard the NASA satellites Terra and Aqua, by an example from Lake Maracaibo, Venezuela. The MODIS instrument has moderate resolution bands of 250 m and 500 m and a wide spectral range. This allows the MODIS instrument to provide images of daylight-reflected solar radiation and day/night time thermal emissions. The MODIS instrument was originally designed for land imaging, and with medium resolution it also shows potential for daily monitoring of the coastal zones looking for oil spills. Cloud cover and the lack of sun light limits the use of optical sensors. On the other hand, multiple wavelengths can give additional information to distinguish slicks produced by algal blooms from oil spills. Yet it is difficult to establish automated feature recognition systems that identify oil spills as external knowledge about the region, environment and current events is needed in the visual analysis of the satellite images to discriminate between various events.

Hyperspectral sensors used for oil spill monitoring have a potential for detailed identification of materials and better estimation of their abundance.

With more than 200 wavelengths provided by a hyperspectral sensor, the spectral signature of oil can be exploited and used to distinguish between different oil types (crude or light oil). This can also eliminate the false alarm rate of ocean features that have the same colour and appearance as oil. Salem and Kafatos (2001) found that a signature matching method based on airborne hyperspectral imaging (looking at chemical composition) is more accurate than the conventional techniques, where analysis is based on visual interpretation of the oils colour and its appearance in the satellite image. There is currently no commercial space-borne hyperspectral sensor in orbit. The NASA EO-1 Hyperion hyperspectral sensor is an example of a space-borne technology demonstrator that was launched in 2000. However, its major drawback is its small swath width of only $7.5 \times 100$ km.

Oil absorbs solar radiation and re-emits a portion of this energy as thermal energy. IR sensors observe thick oil slicks as hot, intermediate thickness of oil as cool, while thin oil is not possible to detect (Fingas & Brown, 1997). At night a thick spill can appear cooler than the water since it releases heat quicker than its surrounding water (Tseng & Chiu, 1994). Tseng and Chiu examined the use and capability of the visible and IR sensors of NOAA Advanced Very High Resolution Radiometer (AVHRR) for early detection and monitoring of oil spills. Oil spills from the 1991 Persian Gulf war were studied. Thick and thin oil layers and the boundary between water and oil were possible to detect by the IR channel, but the oil spills may not have a significant different temperature signature from the surrounding water at night. Oil spills could be detected in the visible images only under highly favourable lighting and sea conditions.

UV technology can be used to detect oil spills as the spill displays high reflectivity of UV radiation even at thin layers. The UV instrument is not usable at night, and wind slicks, sun glints and biogenic material can cause false alarms in

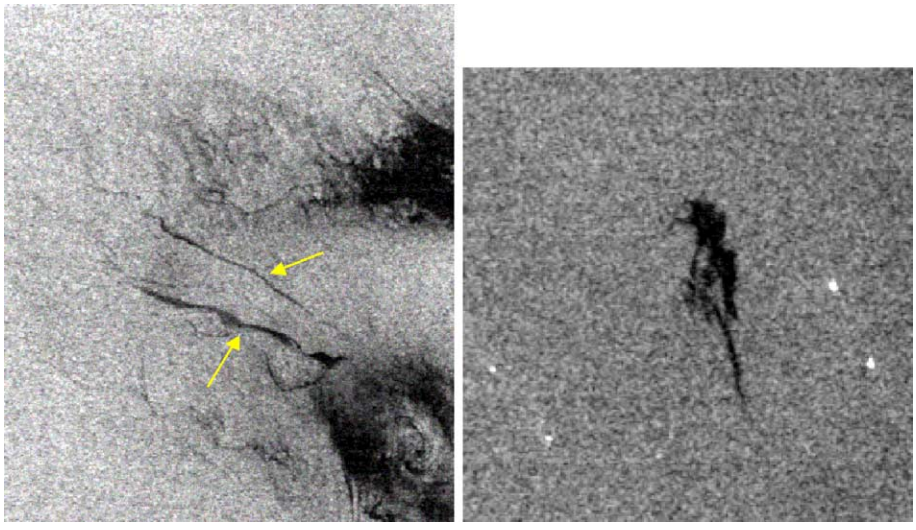

Fig. 1. Two subscenes of an ENVISAT ASAR Wide Swath Mode (WSM) image from the German Baltic Sea (7th of August 2003). Left: The two slicks, indicated by yellow arrows, were classified as algae by a German surveillance aircraft. Several other phenomena (possible low wind) causing low backscattering are visible in the scene. The size of the subscene is 346×405 pixels. Right: The slick was classified as alga by a German surveillance aircraft. The size of the subscene is 236×241 pixels. ©ESA/KSAT 2004.

the UV data. These interferences are often different from those for IR, and a combination of IR and UV can provide a more reliable indication of oil and can be used for estimating oil thickness (Fingas & Brown, 1997).

A MWR is another passive sensor. The instrument looks at the microwave radiation in the wavelength cm to mm range that the ocean emits, and therefore is almost weather-independent (Trieschmann et al., 2003). Oil slicks emit stronger microwave radiation than the water and appear as bright objects on a darker sea. According to Robinson (1994), oil slicks can have strong surface-emissivity signatures, but as a spatial resolution of tens to hundreds of meters is desirable for the determination of oil slicks, this type of sensors for oil spill thickness monitoring is most appropriately pursued by aircraft sensor. Zhifu et al. (2002) did some experiments using airborne (AMR-OS) and a ship borne (K-band) MWRs looking at various oil types and thickness. They found that MWRs are useful tools for measuring the thickness and estimating the volume of the spills, but the resolution is not fine enough to give accurate results. Fingas and Brown (1997) summarize studies done on this field and conclude that the potential of radiometers as a reliable device for measuring slick thickness is uncertain.

RADARSAT-1 and Landsat-5/Thematic Mapper (TM) were used to capture images of the Guanabara Bay, Brazil, after an oil spill emergency where a pipeline ruptured (Bentz & de Miranda, 2001). Bentz and de Miranda found that RADARSAT-1 provided suitable temporal coverage, while cloud cover, haze and the 8-day revisit schedule (using both Landsat-5 and -7) prevented Landsat from being used systematically for oil spill monitoring. However, many sea surface temperature and ocean colour sensors have a large swath width and can provide daily coverage of the earth surface (e.g. the revisit time for MODIS is 2 days and for SeaWiFS 1 day).

In summary, SAR is still the most efficient and superior satellite sensor for oil spills detection, though it does not have capabilities for oil spill thickness estimation and oil type recognition. SAR is useful particularly for searching large areas and observing oceans at night and at cloudy weather conditions. Usually even small volumes of oil cover large areas (several hundred meters) and thus the need for very high spatial resolution in SAR images is not crucial. Bern et al. (1992a), Wahl et al. (1994a, 1996) found Low Resolution ERS-1 SAR images with a spatial resolution of 100 m sufficient for oil spill detection. The original ERS images were filtered using a 5×5 mean filter, which gave better noise characteristics than the full resolution images, and they were therefore easier to analyse. SAR also has some limitations, as a number of natural phenomena can give false oil spill detections. In addition, SAR is only applicable for oil spill monitoring in a certain range of wind speeds. The usefulness of SAR in terms of responding to oil spills at various conditions is covered in more detail in the next section.

## 3. Detectability of oil spills in SAR images

Oil slicks dampen the Bragg waves (wavelength of a few cm) on the ocean surface and reduce the radar backscatter coefficient.[2] This results in dark regions or spots in a satellite SAR images. Fig. 2 gives two examples.

Kotova et al. (1998) emphasises the importance of *weathering processes*,[3] as they influence oil spills physicochemical properties and detectability in SAR images. The processes that play the most important role for oil spill detection are evaporation, emulsification and dispersion. Lighter components of the oil will evaporate to the atmosphere. The rate of evaporation is dependent on oil type, thickness of the spill, wind speed and sea temperature. Emulsification is estimated based on water uptake as a function of the wind exposure of the actual oil type. Dispersion is an important factor in deciding the lifetime of an oil spill and it is strongly dependent on the sea state.

### 3.1. Discrimination between oil spills and look-alikes

A part of the oil spill detection problem is to distinguishing oil slicks from other natural phenomena that dampen the short waves and create dark patches on the surface. Natural dark patches are termed oil slick *look-alikes*. Oil slicks may include all oil related surface films caused by oil spills from oilrigs, leaking pipelines, passing vessels as well as bottom seepages, while look-alikes do include natural films/slicks,[4] grease ice, threshold wind speed areas (wind speed <3 m/s), wind sheltering by land, rain cells, shear zones, internal waves, etc. (Espedal, 1998). Oil spills in a narrow sense are only man-made slicks associated with crude petroleum and its products, heavy and light fuel. Fig. 3 shows an example of a dark spot detected as oil spill by three different satellite-based analysis systems while verified as look-alike by aircraft.

The fact that the radar cross-section values for oil spills are not unique poses a problem in the development of an oil spill detection and monitoring system (Hovland & Johannessen, 1994). Natural films can be very difficult to distinguish from oil spills. Examples are presented in Hovland and Johannessen (1994). Due to a higher viscosity than natural films, oil spills tend to remain more concentrated and in turn provide larger dampening. In Espedal (1998), some trends in slick properties were found for oil

[2] Normalized Radar Cross Section (NRCS) ($\sigma_0$): The normalised measure of the radar return from, e.g. the ocean is called the radar backscatter coefficient, or sigma nought. It is defined as the reflective strength of the radar target, $\sigma$, per unit area on the ground, $A$: $\sigma_0=\sigma/A$ (Curlander & McDonough, 1991). (How to derive the $\sigma_0$ value from the RADARSAT-1, ERS-1 and -2 SAR products is described in Laur et al. (2002) and Shepherd (2000)).

[3] Weathering processes include: spreading, drift, evaporation, dissolution, dispersion, emulsification, sedimentation, biodegradation and photo-oxidation (Kotova et al., 1998).

[4] Natural film: microlayer of organic substances secreted by fish and several planctonic species (Hovland et al., 1994).

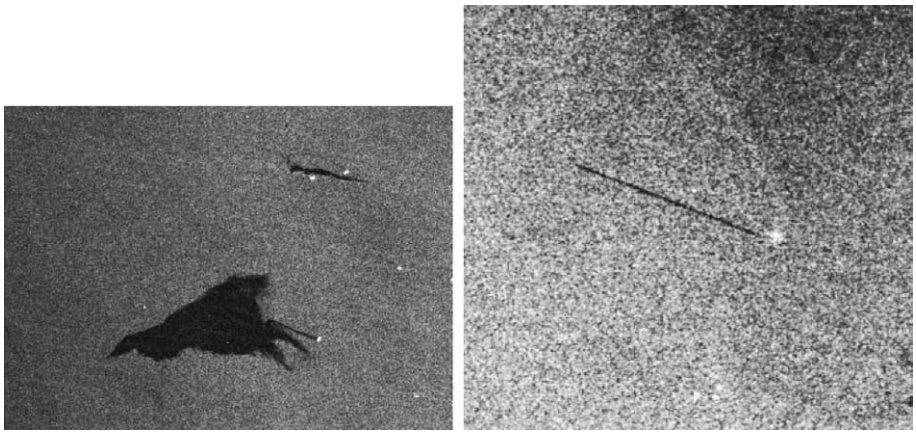

Fig. 2. Left: A subscene of a RADARSAT-1 ScanSAR Narrow (SCN) near range mode image (30th of July 2002) containing two oil spill examples (classified as oil spill by manual inspection) on a homogeneous background. The size of the subscene is 1432×1032 pixels. Right: A subscene of an ENVISAT ASAR WSM image (24th of July 2003) containing a linear oil spill (classified as oil spill by manual inspection). The size of the subscene is 337×320 pixels. ©CSA/ESA/KSAT 2004.

spills and natural films, but no one-to-one relationships were discovered. Oil spills are reported to give a dampening to the surrounding sea in the range of 0.6 dB to 13.0 dB, and natural films in the range of 0.8 dB to 11.3 dB. A preliminary version of a conceptual model for distinguishing oil spills from other slicks is proposed in Hovland et al. (1994), and later on in Espedal (1998, 1999).

Even though we here focus on single frequency and single polarization SAR images, it is worth mentioning the possibility of a discrimination algorithm based on differences in multi-frequency and multi-polarization signatures. Maio et al. (2001) propose such an algorithm for discrimination between oil spills and false alarm templates. However, Gade et al. (1996) did some experiments to investigate whether spaceborne L-, C- and X-band multi-polarization SARs are capable of discriminating between films of different chemical properties, and found that discrimination is only possible at low to moderate wind speeds. Differences between polarization signatures (film-covered as well as film-free surfaces) were found only for low wind speeds and small incidence angles.

Results from testing the performance of a semi-automatic oil spill detection algorithm, on 59 ERS-1 SAR images, show that oil spills that are misclassified as look-alikes fall into three main categories (Solberg & Solberg, 1996):

- Thin, piecewise-linear slicks. (These slicks might be caused by moving ships changing direction, or by changes in currents or wind directions affecting oil releases from stationary objects)
- Low-contrast slicks in homogeneous sea.
- Slicks on a very heterogeneous background.

In addition to look-alikes, different kinds of pollution can cause slicks that are detectable in SAR images. Wahl et al. (1994b) give some examples of ERS-1 images of fish oil and diesel, run-off water from an open depository, a controlled chemical spill and drilling fluid from an oil rig. The SAR sensor is currently not capable of distinguishing between the different pollutants. A single SAR frequency is possibly not enough to estimate the thickness of the oil spill, but Jones (2001) found for the large *Sea Empress* oil spill a good correlation between the largest reduction in backscatter and the thickest oil as determined by visual observations for a limited range of wind speeds (ca. 5–6 m/s).

These experiences require some attention when choosing features for discrimination between oil spills and look-alikes. Important features like wind speed, physical, geometrical and geographical parameters must be used to discriminate between oil spills and look-alikes.

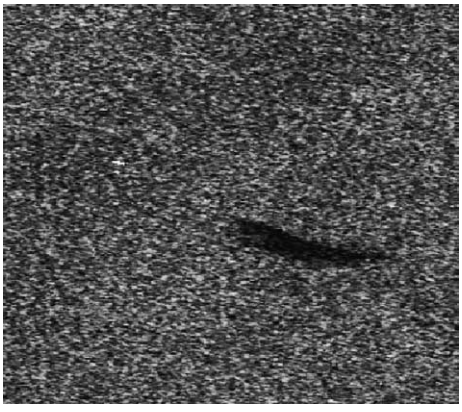

Fig. 3. RADARSAT-1 SCN near range mode subscene (19th of July 2003) containing an oil slick look-alike (at 55,47N, 12,28E) detected as oil spill by Kongsberg Satellite Services AS (KSAT), QinetiQ and Norwegian Computing Center (NR). The size of the subscene is 394×359 pixels. ©CSA/KSAT 2004.

### 3.2. The wind vector

SAR instruments have the advantage over optical sensors that they can acquire images of the oceans and coastal areas

day and night and despite any weather conditions. However, the wind level influences the backscatter level and the visibility of slicks on the sea surface. Oil slicks are visible only for a limited range of wind speeds. Table 2 gives an overview for ERS SAR images. Gade et al. (2000) studied oil spill pollution in the Baltic Sea, the North Sea and the northwestern Mediterranean (700 ERS images). They found that with high wind speed (>10 m/s) few oil spills were detected in the SAR images, which is in agreement with Table 2. They also compared data from airborne surveillance with ERS SAR data. For both sensors they found that the maximum number of detected pollutions was found during summer time, April to September. A reason for this could possibly be that the average wind speed is higher at wintertime at all test sights (e.g. mean wind speed in the North Sea is above 10 m/s). A wind speed between 12 m/s and 14 m/s should possibly be considered as the upper limit for all spaceborne SAR imagery of oil spills (Litovchenko et al., 1999), but the maximum wind speed for slick detection depends on oil type and the age (i.e. time since release) of the spill (Bern et al., 1992a). Thus, an estimate of the wind speed is valuable information for oil spill detection.

For the oil spill detection algorithm described by Solberg et al. (1999), the wind level is set manually based on inspecting the image visually and it is used as input to a threshold procedure. Other possibilities are to incorporate wind information delivered by an external source (e.g. a forecasting centre) or to use automatic methods. With automatic methods for wind estimation, the wind speed can be derived directly from the SAR image. Salvatori et al. (2003) estimate the wind speed from the SAR image by applying an inverted CMOD4[5] model. The wind vector appeared useful in knowing the evolution of the spill and to obtain correct classification.

### 3.3. Satellite configurations for oil spill detection

It is well understood that the radar image is a representation of the backscatter return and mainly proportional to the surface roughness at the scale of the radar wavelength (a phenomenon known as “Bragg scattering”) (Elachi, 1987). The radar backscatter coefficient is also a function of the viewing geometry of the SAR, and the backscatter coefficient decreases with increasing incidence angle. The scattering properties of a material depend on the polarization of the incoming radar signal, and according to Girard-Ardhuin et al. (2003) is the most suitable SAR configuration for slick detection C-band single-polarized VV SAR at incidence angles in the range of 20° to 45°. Dokken (1995) writes that oil spill detection is possible under suitable meteorological conditions when $\sigma_{ocean}$>noise floor+4 dB. Oil spill detection is possible for incidence angles in the range of 20° (lower limit) to the intersection between the $\sigma_{ocean}$ and the noise floor+4 dB (upper limit). Because little multiple reflection of the signal occurs over the ocean, there is little effect on the polarization. It is therefore not much to gain by using cross-polarization (HV or VH) (Robinson, 1994). Fortuny-Guasch (2003) discusses the potential of polarimetric SAR for improved oil spill detection and classification. Its use might extend the validity ranges of wind speed and incidence angles.

Table 2
Visibility of slicks in SAR images (Bern et al., 1992a; Perez-Marrodan, 1998)

| Wind speed (m/s) | Slick signatures |
|---|---|
| 0 | No backscatter from the sea surface, hence no signature of oil slicks. |
| 3 | No impact from the wind on oil slicks. A high probability of oil slick look-alikes due to local wind variations. |
| 3 to 7–10 | Fewer false alarms from local low-wind areas. Oil slicks still visible and more homogeneous background. |
| >7–10 | Only thick oil visible. Thinner oil slicks will be invisible due to a combination of oil spill dispersion. Thick oil can be visible with wind stronger than 10 m/s. |

For RADARSAT-1, Vachon et al. (1998) recommend the SCN near range mode (see Table 3) for slick detection. ScanSAR Wide (SCW) can cause limitations because of the poor resolution of 100 m. RADARSAT-1 is not particularly suited for oil spill detection because of its HH polarization, as predictions show that oil spill detection will not be possible for the largest incident angles especially at low wind speeds (Wahl et al., 1994a). However, it is successfully used in operating oil spill monitoring. No significant difference in practical performance between the detection capabilities of RADARSAT-1 versus ENVISAT has yet been reported for operational use; however, the experience might still be limited (see also Shepherd et al., 2004). ENVISAT’s ASAR WSM covers a much wider swath than its predecessors ERS-1 and -2, but the resolution is significantly lower. From Table 3 we can see that there is a trade-off between image resolution and swath coverage. Generally, for efficient oil spill monitoring larger swath widths should be chosen on the expense of somewhat lower resolution.

Since the SAR satellites usually have polar orbits, the coverage depends on the latitude. Coverage is good in the polar regions and decreases with the distance from the poles. For the Mediterranean Sea the number of satellites passes per day is 0.04 for ERS, 0.27 for RADARSAT-1 (SCN near range) and 0.36 for ENVISAT (Wide Swath Mode) (Perez-Marrodan, 1998). As the visibility of oil spills reduces with time (e.g. the rate of natural dispersion at moderate wind speed conditions is about 0.5–2% of the oil volume/hour (Kotova et al., 1998)) and an early warning is wanted, a high number of passes per day is favourable. With steerable antennas, like the one planned for the RADARSAT-2 SAR, we get more flexible observation possibilities and thus less dependent, e.g. on the repeat cycles of the satellites.

[5] CMOD4: developed by ESA for wind vector evaluation of C-band scatterometer.

Table 3
Examples of satellite modes

| SAR sensor | Mode | Resolution (m) | Pixel spacing (m) | Swath width (km) | Incidence angle (°) |
|---|---|---|---|---|---|
| ERS-2 | PRI | 30×26.3 | 12.5×12.5 | 100 | 20–26 |
| ENVISAT | Image Mode (Precision Image) | 30×30 | 12.5×12.5 | 100 | 15–45 (7 swaths) |
| RADARSAT-1 | SCN | 50×50 | 25×25 | 300 | 20–46 |
| RADARSAT-1 | SCW | 100×100 | 50×50 | 450–500 | 20–49 |
| ENVISAT | WSM | 150×150 | 75×75 | 400 | 16–44 |

Approximate values are given. Product overviews: RADARSAT International (2000), European Space Agency (2002) and ERS-2 Web-site (2004). Precision Image Mode (PRI).

These are all important factors in estimating the usefulness and efficiency of the SAR, and in designing future satellite missions for pollution monitoring.

### 3.4. Speckle noise

Speckle arises because the resolution of the sensor is not sufficient to resolve individual scatters within a resolution cell. Speckle is a large problem in SAR images since even a homogeneous area has a statistical distribution with large standard deviation. Incoherent averaging multiple looks may reduce speckle[6] (Leberl, 1990). Another possibility is to smooth the speckles after the image has been formed. Barni et al. (1995) tested two types of filters, general noise-reducing filters that do not assume any a priori speckle model and adaptive filters assuming a multiplicative speckle model (speckle noise by a multiplicative model is described by Lee (1981)). Better results were reported for the latter type in their oil spill detection algorithm.

For oil spill applications, a filter should suppress speckle noise, but still preserve small and thin oil spills.

## 4. Methodology for oil spill detection in SAR images

We distinguish between manual approaches and automatic algorithms for oil spill detection. Detection of oil spills can be divided in (Indregard et al., 2004):

- Detection of suspected slicks.
- Manual verification of the slicks (oil/look-alike) and assignment of confidence levels.

This section addresses issues regarding the design of oil spill detection systems.

### 4.1. Manual inspection

Since 1994 KSAT in Norway has provided a manual oil spill detection service. Here operators are trained to analyse SAR images for the detection of oil pollution. The KSAT approach is described by Indregard et al. (2004). External information about wind speed and direction, location of oilrigs and pipelines, national territory borders and coastlines are used as support during the analysis. The operator uses an image viewer that can calculate some spot attributes, but he/she still has to go through the whole image manually. This is time consuming. Possible oil spills found are assigned either high, medium or low confidence levels. The assignment is based on the following features: the contrast level to the surroundings, homogeneity of the surroundings, wind speed, nearby oilrigs and ships, natural slicks near by, and edge and shape characteristics of the spot. The determination of a confidence level is not exact science and there will always be an uncertainty connected to the results from manual inspection.

### 4.2. Manual detection compared to automatic detection

During manual inspection, contextual information is an important factor in classifying oil spills and look-alikes. A challenge is to somehow incorporate the "expert knowledge" into the automatic algorithm. In Solberg and Volden (1997), a set of rules and knowledge about external conditions (e.g. wind speed) are used to adjust prior probabilities of oil slicks in the scene. This information is incorporated into a classifier based on a multivariate probability distribution function.

Fiscella et al. (2000) found that a human image interpreter and a classification algorithm have similar ability to discriminate oil spills from look-alikes, but the image set used contained only 21 oil spill candidates.

A study of best practise, based on a comparison of KSAT's manual approach, NR's automatic algorithm (described in Bjerde et al., 1993; Solberg & Solberg, 1996; Solberg & Volden, 1997 and lately in Solberg et al., 1999, 2003) and QinetiQ's semi-automatic oil spill detection approach, has been performed by the ongoing Oceanides project (Indregard et al., 2004). QinetiQ's semi-automatic approach covers only the first step of an automatic algorithm, dark spot detection, and therefore the output targets must be classified visually by an operator. In this study the three satellite-based approaches were compared to airborne verifications in a satellite-airborne campaign. The study was done without the operators or the algorithms knowing of the aircraft verifications. (The benchmark set

[6] The bandwidth of the SAR system is divided into $N$ discrete contiguous segments, each segment generating a single-look lower resolution image. The intensities of the $N$ single-look images are incoherently averaged to form a multiple-look image (Ulaby et al., 1986).

consisted of 32 RADARSAT-1 images.) This data set contained 17 verified oil spills. KSAT detected 15 of these slicks, NR's algorithm detected 14, and QinetiQ detected 12. The results show that a challenge is to have all operators pick out the same spots and assign the same confidence levels. NR's algorithm is objective (with one exception of manual wind level assignment, see Section 3.2) and produces the same result repeatedly. Good agreement was found for high-contrast slicks among the various methods, but there were some differences on low-contrast slicks. The operators at KSAT use 3–25 min to analyse a scene (on average 9 min), the NR's algorithm used about 3 min and QinetiQ's algorithm used 20 min per scene in average. This shows that automatic approaches are more feasible as the volume of SAR data grows.

### 4.3. Design issues for automatic detection systems

Kubat et al. (1998) identified a number of issues during their development of a machine learning component for an oil spill detection system. The first issue is the *scarcity of data*, as most satellite SAR images acquired contain no oil spills. The second is the *imbalanced training set*. Oil spill detection is an application where the classifier should detect a rare but important event (look-alikes appear much more frequent). Oil spills happen to appear in *batches*, where examples drawn from the same image constitute a single batch. A similarity within batches and dissimilarity between batches can be present, which can influence the classifier training. And finally, the *performance* of the classifier relates to the users' possibility to decrease the number of alarms at the expense of missing genuine oil spills (specificity). Indregard et al. (2004) also point out that automatic algorithms should be tuned in order to be certain that no suspicious oil spills that would be detected by an operator are missed.

The significant differences in mode characteristics for different SAR sensors, as presented by Table 3, suggest a development of sensor specific modules.

All of these are considerations to be taken into account when designing an automatic system for oil spill detection.

## 5. Automatic techniques for oil spill detection in SAR images

Several of the published papers on oil spill algorithms for SAR images (e.g. Fiscella et al., 2000; Frate et al., 2000; Solberg et al., 1999) describe a structure comparable with the one in Fig. 4.

The importance of the wind vector was emphasised in Section 3.2, and Salvatori et al. (2003) include two additional steps of wind direction estimation and wind speed calculation. Manual wind estimation was included by Solberg et al. (1999). SAR image calibration, land masking, speckle reduction and class signature databases belong in this framework as well, but Fig. 4 shows the core modules of an oil spill detection and classification algorithm. This section covers algorithms and techniques related to each module of Fig. 4.

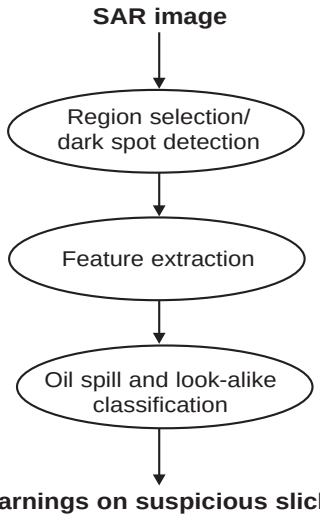


Fig. 4. A framework for oil spill detection algorithms.

### 5.1. Segmentation techniques

As oil spills are characterised by low backscattering levels, these suggest the use of thresholding for dark spot segmentation. An early attempt on segmentation of ERS-1 SAR images is described by Skøelv and Wahl (1993). The algorithm simply looks for bimodal histograms in widows of size $N \times N$ pixels ($N$ was sat to 25 pixels). This is reported as a good method for detection of oil spills provided that the spill is not to thin. A similar approach is briefly described in Vachon et al. (1998) and Manore et al. (1998). This algorithm, which is developed for RADARSAT-1 SAR data, spatially averages the image before a user-defined adaptive threshold is applied. As both these algorithms lack a classification step look-alikes will be detected as well.

Solberg et al. (1999, 2003) apply an adaptive algorithm where the threshold is sat $k$ dB below the mean value estimated in a moving window. The thresholding is combined with a multiscale pyramid approach and a clustering step to better separate the spill from its surroundings. Noise reduction by a mean filter smoothes the edges.

The use of hysteresis thresholding was introduced by Canny (1986) and is applied by Kanaa et al. (2003) for detecting oil spills in ERS amplitude images. A search is done in the eight neighbourhood directions followed by a merging step of the responses. Linear features are reported accentuated by this method.

An oil slick detection approach, based on the Laplace of Gaussian (LoG) and Difference of Gaussian (DoG) operators, is described in Change et al. (1996) and Chen et al. (1997). The LoG operator is applied on the coarsest layer of

a 2×2 pixel reduced pyramid with three layers. The concave areas of the grey level surface are selected. The DoG is used to locate those areas with more than half of the slick boundary pixels greater than $\mu+1.75\sigma$ (as selected for ERS-1, where $\mu$ and $\sigma$ are mean and standard deviation over all image pixels, respectively). To improve the result the finer layers of the pyramid are processed.

The use of wavelets in ocean feature detection (including oil spills) is described by Liu et al. (1997) and Wu and Liu (2003). In the general linear feature detection scheme, the analysing wavelet is defined as the LoG. Regions with multiple histogram peaks are selected for the wavelet transform. The wavelet is applied as an edge detector as the contours of the zero crossing indicates the feature edges (see Canny, 1986).

As oil spills dampens the capillary waves, Mercier et al. (2003) suggest a segmentation method based on detecting local variations of the wave spectra. First a multi-resolution analysis is achieved by a wavelet packet transform then a Hidden Markov Chain (HMC) model is applied to the wavelet coefficients. The technique is tested on an ERS PRI image.

QinetiQ's dark spot algorithm uses a Constant False Alarm Rate (CFAR) algorithm to locate dark regions. The dark spots are merged according to a clustering radius and a threshold, and the Hough transform is used specially to identify linear targets (Indregard et al., 2004).

To allow dealing with mixed surface-cover classes and unsharp boundaries among regions, Barni et al. (1995) propose an algorithm based on fuzzy clustering. A membership function $u_A(x)$ is assigned to each pixel $x$, which measures how much the pixel belongs to a set A. The Fuzzy C-means (FCM) algorithm is applied, and a pyramid structure is used in finding the membership values. Uncertain pixels are tested in the lower pyramid level. Neighbouring regions are identified, and a Sobel operator is used to enhance the main edges of the original filtered image. Regions, whose common border does not have a high enough percentage of large gradient points, are merged together. One difficulty with fuzzy clustering is to find the optimum number of clusters.

A method using mathematical morphology for oil spill segmentation is presented by Gasull et al. (2002). Combinations of opening and closing[7] operations are used for oil spill filtering and thresholding. The algorithm aims at detecting spills from sailing tankers, and some features used are the elongatedness and dampening of the spill.

Even though a variety of methods are applied, the common goal is to detect all suspicious slicks and to preserve the slick shapes. The latter is of most importance for the success of discriminating oil spills from look-alikes in the following steps.

[7] Opening: erosion followed by dilation. Closing: dilation followed by erosion (see Sonka et al., 1999 for an introduction to mathematical morphology).

### 5.2. Slick feature extraction

From the thresholded dark spot image, feature extraction is used to compute features for each slick. Table 4 summarizes the features used in three different algorithms. In a feature vector that is input to the classifier, the individual features are typically covered by the following classes:

- *The geometry and shape of the segmented region.* Geometric and shape features are applied by all methods in Table 4. To detect pollution from sailing tankers cleaning their tanks, an important feature is elongatedness which can be expressed as a ratio between the width and length of the slick (Gasull et al., 2002). Another possible feature useful in identifying these spots is the first invariant statistical moment of Hu (1962).
- *Physical characteristics of the backscatter level of the spot and its surroundings.* Frate et al. (2000) found that features containing most valuable information for classification by neural networks were features covering information on the gradient of the backscattering

Table 4
Features applied by various algorithms

| # | Feature | 1 | 2 | 3 |
|---|---|---|---|---|
| 1 | Slick area ($A$) | × | × | × |
| 2 | Slick perimeter ($P$) | × | | × |
| 3 | $P/A$ | | | × |
| 4 | Slick complexity | × | × | |
| 5 | Spreading (low for long thin slicks, high for circular shape) | × | | |
| 6 | Slick width | | × | |
| 7 | First invariant planar moment (Hu, 1962) | | × | |
| 8 | Dispersion of slick pixels from longitudinal axis | | | × |
| 9 | Object/dark area standard deviation | × | | × |
| 10 | Background/outside dark area standard deviation | × | | × |
| 11 | Max contrast (between object and background) | × | | |
| 12 | Mean contrast (between object and background) | × | | |
| 13 | Max border gradient | × | | |
| 14 | Mean border gradient | × | × | |
| 15 | Gradient standard deviation | × | | |
| 16 | Local area contrast ratio | | × | |
| 17 | Power-to-mean ratio of the slick | | × | |
| 18 | Homogeneity of surroundings | | × | |
| 19 | Average NRCS inside dark area | | | × |
| 20 | Average NRCS in limited area outside dark area | | | × |
| 21 | Gradient of the NRCS across the dark area perimeter | | | × |
| 22 | Ratio #9 to #10 | | | × |
| 23 | Ratio #19 to #9 | | | × |
| 24 | Ratio #20 to #10 | | | × |
| 25 | Ratio #23 to #24 | | | × |
| 26 | Ratio #19 to #20 | | | × |
| 27 | Distance to a point source | | × | |
| 28 | Number of detected spots in the scene | | × | |
| 29 | Number of neighbouring spots | | × | |

1: Frate et al. (2000); 2: Solberg et al. (1999); 3: Fiscella et al. (2000). × indicates that the parameter is used in the feature vector of the particular algorithm.

value when passing from background to spill (#13, #14 and #15). In addition, the background standard deviation (#10) was found important which is a parameter highly affected by the wind level and is generally high for natural sea slicks. Similarly in Fiscella et al. (2000), features connected to the background surrounding the slick were found to be important due to the wind speed dependence of oil spill observations (these features could also be classified as contextual features).

- *Spot contextual features.* Examples are slick location relative to the shore and distance to ships and oilrigs. In the contextual analysis of the supervised discrimination algorithm described by Espedal (1999) is a "hot-spot" pollution source database used. Improved classification results were found by Solberg and Volden (1997) when the dark spots are classified in the context of their surroundings and weather information is incorporated. Espedal and Wahl (1999) suggest using wind history information for slick classification and slick age estimation. Wind history can also be looked at as an indirect spot feature.
- *Texture.* In contradiction to the pixel intensity itself, texture provides information about the spatial correlation among neighbouring pixels. Assilzadeh and Mansor (2001) describe an early warning system where texture features based on grey level co-occurrence matrixes (GLCM)[8] are used. Homogeneity and angular second moment were found effective in separation of oil spills from other objects. Power-to-mean ratio of the slick and the surroundings is used by Solberg et al. (1999) as a measure of homogeneity.

Even though the different methods in Table 4 do not apply the exact same features, several of the features are different measures of the same characteristic.

Fractal texture description can be used to describe natural surfaces (Pentland, 1984). The use of fractal dimension[9] as a feature for classifying observed ocean radar signatures is suggested in Gade and Redondo (1999). A box-counting algorithm (the method is described in Keller et al., 1989) is used to find the fractal dimension $D$. A difference in $D$ of oil spills compared to other oceanic phenomena is reported. In another paper on fractal dimension by Benelli and Garzelli (1999) was a steady fractal dimension value of $D$=2.45 found for the sea surface, while an average value of $D$=2.15 was found for oil spills. A smaller $D$ indicates less roughness.

Good features are important, but the lack of good guidelines on how to acquire them has been pointed out by Kubat et al. (1998).

### 5.3. Classification methods

As a number of phenomena can create dark patches in a SAR image, the purpose of the classifier is to distinguish oil spills from the other cases.

Based on results from selecting the dark regions with a NRCS lower than one half of the average NRCS of the sea area in the image, Fiscella et al. (2000) apply a Mahalanobis classifier to estimate the probability $p$ of a dark spot being an oil spill. For ERS images, $p$>2/3 and not looking at uncertain cases, 93% of the oil spills were correctly classified (a priori) and 82% of the oil spills in the test set were correctly classified. This was compared with a compound probability classifier. Here $p$>2/3 gave a 85% correct classification rate (a priori) of oil spills and 91% of the oil spills in the test set were correctly classified. A training set of 80 oil spills and 43 look-alikes and a test set of 11 oil spills, 4 uncertain and 6 look-alikes were used.

In Solberg et al. (1999) is a probability assigned to a spot from a multivariate Gaussian density function. The unknown parameters are derived from a signature database. (Fiscella et al.'s method is in a similar way based on previous measurements.) This is combined with a prior model for the number of look-alikes, a model for the presence of a slick in the vicinity of a bright object and a rule-based modification of the probability density to take into account feature combinations that are indications of certain scene conditions. The leave-one-out method with 84 scenes gave a correct classification of 94% for oil spills.

An artificial neural network (NN) is a mathematical model composed of many neurons[10] operating in parallel. An approach for oil spill detection, tested on ERS images, based on a multilayer perceptron (MLP) neural network with two hidden layers is described by Frate et al. (2000). Selection of a dark object and image fragmentation is performed with manual interaction, while feature extraction and classification into oil spill or look-alike is performed automatically. The input (to the net) is also here a feature vector. The neuron is the elemental building block of each layer in the net, and it is mainly characterized by an activation function (in this case a non-linear sigmoid function). The neuron computes the sum of its inputs, adds a bias term, and drives the result through the activation function. A single output is produced from each neuron. Using the leave-one-out method with 139 sample oil spills, 18% were reported misclassified as look-alikes.

The proposed automatic methods for oil spill detection discussed here report accuracies from 82% to 94% correct classification of oil spills. These studies are however performed on different data sets, and the approaches differ both in terms of segmentation approach, feature extraction methods, and classification methodology. The most impor-

[8] GLCM: approximates the grey level joint probability distribution (Haralick, 1979).

[9] A surface fractal dimension corresponds closely to our intuitive notion of roughness (Pentland, 1984).

[10] A neuron is a non-linear computational element connected to other neurons by links characterized by different weights (see also Bishop, 1995).

tant steps in this process are segmentation and feature extraction. If a slick is not detected during segmentation, it cannot be classified correctly. If the features have good discriminatory power, the classification problem will be easier and several classifiers will work. We believe that the variance in shape, contrast, and surroundings of oil slicks and look-alikes is so large that it is necessary to subdivide the problem into subclasses, and to guide the classifier by using as much prior information about the problem as possible. This was done in the approach presented in Solberg et al. (1999), which is the approach with the highest accuracy reported so far.

## 6. Conclusion and suggestions for further work

Synthetic aperture radar is the most applicable spaceborne sensor for operational oil spill detection, mostly because of its all-weather/all-day detection capabilities and wide coverage. It can operate from light wind to wind speeds up to 12–14 m/s, but the maximum wind speed for oil slick detection depends on oil type and age. Sensors operating in wide swath mode with a spatial resolution of 50–150 m are found to be sufficient and allow covering large ocean areas efficiently.

The largest challenge in detection of oil spills in SAR images is accurate discrimination between oil spills and look-alikes. Most low wind situations can be handled by analysing the surroundings of a slick, but natural films cannot always be properly distinguished from oil spills based on a SAR image alone. Additional information about algal blooms is desired, particularly for the Baltic Sea, where alga is common during the summer. Such information can be derived from optical sensors. Future oil spill systems should incorporate alga information either from multisensor studies, or by using prior knowledge about the likelihood of observing alga in a given area at a certain time of the year.

For operational purposes, there is a need for coordination between satellite overpasses and aerial surveillance flights. Presently, aerial surveillance is needed for collecting evidence to prosecute the polluters. The combination of coordinated satellite image acquisitions and aerial surveillance flights is presently used operationally by many countries in Northern Europe. Many of these services use the KSAT manual approach to identify oil spills from the satellite images.

Future SAR missions are crucial for sustainable operational oil spill detection services. There is a number of commercial SAR missions planned; the Japanese Advanced Land-Observing Satellite (ALOS) and the European TerraSAR-L are both satellites with L-band SAR, which means an increased wavelength (24 cm) compared to, e.g. ERS and ENVISAT. TerraSAR-X and COSMO/SkyMed (dual use) are German and Italian X-band satellites. TerraSAR-X will have a best resolution of 1 m, but will also provide a ScanSAR mode with 16 m resolution and 100 km swath width. Concerning oil spill detection, the most promising of the coming missions is RADARSAT-2 with its C-band SAR. RADARSAT-2 is planned launched in 2005, and will provide improved resolution and flexibility in selection of polarization options (both single and full polarization modes will be available). A future spaceborne C-band SAR to replace ENVISAT ASAR would be needed to sustain the quality of the oil spill detection services. This is acknowledge by ESA, as many other ocean applications use C-band SAR images regularly.

A study of best practice of manual versus automatic oil spill systems showed that operators show some variance in detecting spills, particularly in assigning an oil spill confidence estimate. An automatic algorithm with a reliable and objective oil spill confidence estimate would be highly desirable. The need for automatic algorithms depend on the number of images to be analysed, but for monitoring large ocean areas it is a cost-effective alternative to manual inspection.

More work on the direct comparison of the performance of manual versus automatic methods for oil spill detection is needed. Up to now, the automatic systems have been tested off-line, thus, additional spills reported by the automatic systems cannot be verified. We still believe that the slicks classified as oil by automatic algorithms should go through a manual inspection prior to sending out aircrafts. In that case, inspection of a couple of slicks per scene would be much more efficient than inspection of the complete scene as currently done. As part of the ESA project Northern View, NR's automatic algorithm will be deployed in KSAT's operational environment.

Automatic oil spill detection algorithms are normally divided into three steps, dark spot detection, dark spot feature extraction, and dark spot classification. Few papers are published on automatic algorithms for classification of oil spills and its look-alikes as most authors focus on the detection step. Large-scale classification studies with acceptable classification performance are reported based on statistical classification (Fiscella et al., 2000; Solberg et al., 1999), and neural nets (Frate et al., 2000). An extensive comparison of the classifiers used by the different approaches, based on the same data set of features, would be desirable.

To increase the performance further, incorporation of more knowledge is needed. We believe that the future oil spill system should be an integrated system, including automatic algorithms, a database of "hotspots" (e.g. oilrigs, sunken ships and seepages), ship lanes, alga information, and more extensive use of wind information.

## Acknowledgements

This work is performed as a part of a PhD study funded by the Norwegian Research Council and the Norwegian Defence Research Establishment. The authors would like to

thank the Oceanides project, in particular KSAT, for the SAR scenes used for illustration purposes.

## References


Assilzadeh, H., & Mansor, S. B. (2001). Early warning system for oil spill using SAR images. *Proc. ACRS 2001—22nd Asian Conference on Remote Sensing, 5–9 November 2001, Singapore*, *vol. 1* (pp. 460–465).

Barni, M., Betti, M., & Mecocci, A. (1995). A fuzzy approach to oil spill detection on SAR images. *Proc. IGARSS '95*, *vol. 1* (pp. 157–159).

Benelli, G., & Garzelli, A. (1999). Oil-spills detection in SAR images by fractal dimension estimation. *Proc. IGARSS'99*, *vol. 1* (pp. 218–220).

Bentz, C., & de Miranda, F. P. (2001). Application of remote sensing data for oil spill monitoring in the Guanabara Bay, Rio de Janeiro, Brazil. *Proc. IGARSS'01*, *vol. 1* (pp. 333–335).

Bern, T. -I., Moen, S., Wahl, T., Anderssen, T., Olsen, R., & Johannessen, J. A., (1992a). Oil spill detection using satellite based SAR. Completion report for Phase 0 and 1. Tech. rep., OCEANOR report no. OCN-R92071, Trondheim.

Bern, T. -I., Wahl, T., Anderssen, T., & Olsen, R. (1992b, 4–6 November). Oil spill detection using satellite based SAR: Experience from a field experiment. *Proc. 1st ERS-1 Symposium, Cannes, France* (pp. 829–834).

Bishop, C. M. (1995). *Neural networks for pattern recognition*. Oxford University Press.

Bjerde, K. W., Solberg, A. H. S., & Solberg, R. (1993). Oil spill detection in SAR imagery. *Proc. IGARSS'93*, *vol. 3* (pp. 943–945).

Canny, J. (1986). A computational approach to edge detection. *IEEE Transactions on Pattern Analysis and Machine Intelligence, PAMI*, *8*(6), 679–698.

Change, L. Y., Chen, K., Chen, C., & Chen, A. (1996). A multiplayer-multiresolution approach to detection of oil slicks using ERS SAR image. *Proc. ACRS 1996—17th Asian Conference of Remote Sensing, Sri Lanka*.

Chen, C. F., Chen, K. S., Chang, L. Y., & Chen, A. J. (1997). The use of satellite imagery for monitoring coastal environment in Taiwan. *Proc. IGARSS'97*, *vol. 3*. (pp. 1424–1426).

Curlander, J. C., & McDonough, R. N. (1991). *Synthetic aperture radar, systems and signal processing. Wiley series in remote sensing*. John Wiley & Sons.

Dokken, S. T. (1995). Optimal bruk av avanserte radarsatellitter. Master's thesis, Institutt for Tekniske Fag, Norges Landbrukshøgskole.

Elachi, C. (1987). *Introduction to the physics and techniques of remote sensing*. John Wiley & Sons.

ERS-2 Web-site. (2004). http://earth.esa.int/services/pg/pgerssarpri.xml, accessed 20 October 2004.

Espedal, H. (1999). Detection of oil spill and natural film in the marine environment by spaceborne SAR. *Proc. IGARSS'99*, *vol. 3* (pp. 1478–1480).

Espedal, H. A. (1998). Detection of oil spill and natural film in the marine environment by spaceborne synthetic aperture radar. PhD thesis, Department of Physics University of Bergen and Nansen Environment and Remote Sensing Center, Norway.

Espedal, H. A., & Johannessen, O. M. (2000). Detection of oil spills near offshore installations using synthetic aperture radar (SAR). *International Journal of Remote Sensing*, *21*(11), 2141–2144.

Espedal, H. A., & Wahl, T. (1999). Satellite SAR oil spill detection using wind history information. *International Journal of Remote Sensing*, *20*(1), 49–65.

European Space Agency. (1998). Oil pollution monitoring. *ESA brochure: ERS and its applications—Marine*, *BR-128*, 1.

European Space Agency. (2002). ASAR product handbook. Tech. rep., European Space Agancy-ENVISAT Product Handbook, Issue 1.1, 1 December 2002.

Fingas, M. (2001). *The basics of oil spill cleanup*. Lewis Publishers.

Fingas, M. F., & Brown, C. E. (1997). Review of oil spill remote sensing. *Spill Science and Technology Bulletin*, *4*, 199–208.

Fiscella, B., Giancaspro, A., Nirchio, F., Pavese, P., & Trivero, P. (2000). Oil spill detection using marine SAR images. *International Journal of Remote Sensing*, *21*(18), 3561–3566.

Fortuny-Guasch, J. (2003). Improved oil spill detection and classification with polarimetric SAR. *Proc. workshop on Application of SAR Polarimery and Polarimetric Interferometry, ESA-ESRIN Frascati, Italy, January 14–16 2004,* available at http://earth.esa.int/polinsar/pr.html, accessed 1 September 2004.

Frate, F. D., Petrocchi, A., Lichtenegger, J., & Calabresi, G. (2000). *Neural networks for oil spill detection using ERS-SAR data*. *IEEE Transactions on Geoscience and Remote Sensing*, *38*(5), 2282–2287.

Friedman, K. S., Pichel, W. G., Clemente-Colón, P., & Li, X. (2002). GoMEx—an experimental GIS system for the Gulf of Mexico Region using SAR and additional satellite and ancillary data. *Proc. IGARSS'02*, *vol. 6* (pp. 3343–3346).

Gade, M., Alpers, W., & Bao, M. (1996). Measurements of the radar backscattering over different oceanic surface films during the SIR-C/X-SAR campaigns. *Proc. IGARSS'96* (pp. 860–862).

Gade, M., & Redondo, J. (1999). Marine pollution in European coastal waters monitored by the ERS-2 SAR: a comprehensive statistical analysis. OCEANS '99 MTS/IEEE*Riding the Crest into the 21st century*, *vol. 3* (pp. 1239–1243).

Gade, M., Scholz, J., & von Viebahn, C. (2000). On the detectability of marine oil pollution in European marginal waters by means of ERS SAR imagery. *Proc. IGARSS 2000*, *vol. 6* (pp. 2510–2512).

Gasull, A., Fabregas, X., Jimenez, J., Marques, F., Moreno, V., & Herrero, M. (2002, September). Oil spills detection in SAR images using mathematical morphology. *Proc. EUSIPCO'2002, Toulouse, France*, *vol. 1* (pp. 25–28).

Girard-Ardhuin, F., Mercier, G., & Garello, R. (2003). Oil slick detection by SAR imagery: potential and limitation. *Proc. OCEANS 2003*, *vol. 1* (pp. 164–169).

Goodman, R. (1994). Overview and future trends in oil spill remote sensing. *Spill Science and Technology Bulletin*, *1*(1), 11–21.

Haralick, R. M. (1979). Statistical and structural approaches to texture. *Proceedings of the IEEE*, *67*, 786–804.

Hovland, H. A., Johannessen, J. A. (1994). Norwegian surface slick report, Final report to Norwegian Defence Research Establishment and Norwegian Space Centre. Tech. rep., Nansen Environmental and Remote Sensing Center.

Hovland, H. A., Johannessen, J. A., & Digranes, G. (1994). Slick detection in SAR images. *Proc. IGARSS'94*, *vol. 4* (pp. 2038–2040).

Hu, C., Müller-Krager, F. E., Taylor, C. J., Myhre, D., Murch, B., Odriozola, A. L., et al. (2003). MODIS detects oil spills in Lake Maracaibo, Venezuela. *EOS, Transactions, American Geophysical Union*, *84*(33), 313, 319.

Hu, M. -K. (1962). Visual pattern recognition by moment invariants. *IEEE Transactions on Information Theory*, *8*, 179–187.

Indregard, M., Solberg, A., Clayton, P. (2004). D2-report on benchmarking oil spill recognition approaches and best practice. Tech. rep., Oceanides project, European Commission, Archive No. 04-10225-A-Doc, Contract No: EVK2-CT-2003-00177.

Ivanov, A., He, M. -X., Fang, M. -Q. (2002). Oil spill detection with the RADARSAT SAR in the waters of the Yellow and East China Sea: A case study. *Proc. ACRS 2002—23rd Asian Conference on Remote Sensing, November 25–29, 2002, Kathmandu, Nepal*.

Jones, B. (2001). A comparison of visual observations of surface oil with synthetic aperture radar imagery of the Sea Empress oil spill. *International Journal of Remote Sensing*, *22*(9), 1619–1638.

Kanaa, T. F. N., Tonye, E., Mercier, G., Onana, V., Ngono, J., Frison, P., et al. (2003). Detection of oil slick signatures in SAR images by fusion of hysteresis thresholding responses. *Proc. IGARSS'03*, *vol. 4* (pp. 2750–2752).

Keller, J. M., Chen, S., & Crownover, R. M. (1989). Texture description and segmentation through fractal geometry. *Computer Vision, Graphics, and Image Processing*, *45*, 150–166.

Kotova, L. A., Espedal, H. A., & Johannessen, O. M. (1998). Oil spill detection using spaceborne SAR; a brief review. Proc. 27th ISRSE, Tromsø, Norway.

Kubat, M., Holte, R. C., & Matwin, S. (1998). Machine learning for the detection of oil spills in satellite radar images. *Machine Learning*, *30*, 195–215.

Laur, H., Bally, P., Meadows, P., Sanchez, J., Schaettler, B., Lopinto, E., et al. (2002). Derivation of the backscattering coefficient (0 in ESA ERS SAR PRI products. Tech. rep., Document No.: ES-TN-RS-PM-HL09, Issue 2, Rev. 5d, 17. September, European Space Agency (ESA).

Leberl, F. W. (1990). *Radargrammetric image processing*. Artech House.

Lee, J. -S. (1981). Speckle analysis and smoothing of synthetic aperture radar images. *Computer Graphics and Image Processing*, *17*, 24–32.

Litovchenko, K., Ivanov, A., & Ermakov, S. (1999). Detection of oil slicks parameters from ALMAZ-1 and ERS-1 SAR imagery. *Proc. IGARSS'99*, *vol. 3* (pp. 1484–1486).

Liu, A. K., Peng, C. Y., & Chang, S. Y. -S. (1997). Wavelet analysis of satellite images for coastal watch. *IEEE Journal of Oceanic Engineering*, *22*(1), 9–17.

Lu, J. (2003). Marine oil spill detection, statistics and mapping with ERS SAR imagery in south-east Asia. *International Journal of Remote Sensing*, *24*(15), 3013–3032.

Lu, J., Lim, H., Liew, S. C., Bao, M., & Kwoh, L. K. (1999). Ocean oil pollution mapping with ERS synthetic aperture radar imagery. *Proc. IGARSS'99*, *vol. 1* (pp. 212–214).

Maio, A. D., Ricci, G., & Tesauro, M. (2001). On CFAR detection of oil slicks on the ocean surface by multifrequency and/or multipolarization SAR. In *Radar conference, 2001. Proceedings of the 2001 IEEE* (pp. 351–356).

Manore, M. J., Vachon, P. W., Bjerkelund, C., Edel, H. R., & Ramsay, B. (1998). Operational use of RADARSAT SAR in the coastal zone: The Canadian experience. *27th International Symposium on Remote Sensing of the Environment, Tromsø, Norway, June 8–12* (pp. 115–118).

Martinez, A., & Moreno, V. (1996). An oil spill monitoring system based on SAR images. *Spill Science and Technology Bulletin*, *3*(1/2), 65–71.

Mercier, G., Derrode, S., Pieczynski, W., Caillec, J. -M. L., & Garello, R. (2003). Multiscale oil slick segmentation with Markov Chain Model. *Proc. IGARSS'03*, *vol. 6* (pp. 3501–3503).

Oceanides Web-site. (2004). http://oceanides.jrc.cec.eu.int/prestige.html, accessed 13 August 2004.

Pavlakis, P., Sieber, A., & Alexandry, S. (1996, June). Monitoring oil-spill pollution in the Mediterranean with ERS SAR. *ESA Earth Observation Quarterly (52)*.

Pentland, A. P. (1984). Fractal-based description of natural scenes. *IEEE Transactions on Pattern Analysis and Machine Intelligence, PAMI*, *6*(6), 661–674.

Perez-Marrodan, M. (1998). ENVISYS—environmental monitoring warning and emergency management system. *Proc. of the AFCEA Kiev Seminar, 28–29 May* (pp. 122–132).

RADARSAT International. (2000). D4, RADARSAT, data products specification. Tech. rep., Doc. No: RSI-GS-026, RADARSAT International.

Robinson, I. S. (1994). *Satellite oceanography. An introduction for oceanographers and remote-sensing scientists. Wiley–Praxis series in remote sensing.*

Salem, F., & Kafatos, P. M. (2001). Hyperspectral image analysis for oil spill mitigation. *Proc. ACRS 2001—22nd Asian Conference on Remote Sensing, 5–9 November 2001, Singapore*, *vol. 1* (pp. 748–753).

Salvatori, L., Bouchaib, S., Frate, F. D., Lichtenneger, J., & Samara, Y. (2003). Estimating the wind vector from radar SAR images when applied to the detection of oil spill pollution. *Fifth International Symposium on GIS and Computer Catography for Coastal Zone Management, CoastGIS'03.*

Shepherd, I. (2004). Developing an operational oil-spill service in GMES. *Version 2, OCEANIDES workshop, 25 May, 2004, EEA, Copenhagen*, available at: http://intelligence.jrc.it/marine/oceanides/oceanides.html, accessed 23 August 2004.

Shepherd, I., Bauna, T., Chesworth, J., Kourti, N., Lemoine, G., & Indregard, M. (2004). Use of ENVISAT at JRC for marine monitoring in 2003. *JRC Technical Note*, (available at: http://pta.jrc.cec.eu.int/entity.gx/entity.object/SEC–000000000002CB39/entity.name/envisatreport-7.pdf, accessed 23 August 2004).

Shepherd, N. (2000). Extraction of beta nought and sigma nought from RADARSAT CDPF products. Tech. rep., Report No.: AS97-5001, Rev. 4–28 April, Altrix Systems.

Simecek-Beatty, D., & Clemente-Colón, P. (2004). Locating a sunken vessel using SAR imagery: Detection of oil spilled from the SS Jacob Luckenbach. *International Journal of Remote Sensing*, *25*(11), 2233–2241.

Skøelv, Å., Wahl, T. (1993). Oil spill detection using satellite based SAR, Phase 1B competition report. Tech. rep., Norwegian Defence Research Establishment.

Solberg, A. H. S., Dokken, S. T., & Solberg, R. (2003). Automatic detection of oil spills in Envisat, Radarsat and ERS SAR images. *Proc. IGARSS'03*, *vol. 4* (pp. 2747–2749).

Solberg, A. H. S., & Solberg, R. (1996). A large-scale evaluation of features for automatic detection of oil spills in ERS SAR images. *Proc. IGARSS'96*, *vol. 3* (pp. 1484–1486).

Solberg, A. H. S., Storvik, G., Solberg, R., & Volden, E. (1999). Automatic detection of oil spills in ERS SAR images. *IEEE Transactions on Geoscience and Remote Sensing*, *37*(4), 1916–1924.

Solberg, A. H. S., & Volden, E. (1997). Incorporation of prior knowledge in automatic classification of oil spills in ERS SAR images. *Proc. IGARSS'97*, *vol. 1* (pp. 157–159).

Sonka, M., Hlavac, V., & Boyle, R. (1999). *Image processing, analysis, and machine vision*. Brooks/Cole Publishing.

Trieschmann, O., Hunsänger, T., Tufte, L., & Barjenbruch, U. (2003). Data assimilation of an airborne multiple remote sensor system and of satellite images for the North- and Baltic sea. *Proceedings of the SPIE 10th int. symposium on remote sensing, conference* "*remote sensing of the ocean and sea ice 2003*" (pp. 51–60).

Tseng, W. Y., & Chiu, L. S. (1994). AVHRR observations of Persian Gulf oil spills. *Proc. IGARSS'94*, *vol. 2* (pp. 779–782).

Ulaby, F. T., Moore, R. K., & Fung, A. K. (1986). *Microwave remote sensing: Active and passive. Vol. 3: From Theory to Applications*. Artech house.

Vachon, P. W., Thomas, S. J., Cranton, J. A., Bjerkelund, C., Dobson, F. W., & Olsen, R. B. (1998). Monitoring the coastal zone with the RADARSAT satellite. *Oceanology International 98, UK, March 10–13,* 10 pages.

Wahl, T., Anderssen, T., Skøelv, Å. (1994a). Oil spill detection using satellite based SAR, Pilot Operation Phase, final report. Tech. rep., Norwegian Defence Research Establishment.

Wahl, T., Skøelv, Å., & Andersen, J. H. S. (1994b). *Practical use of ERS-1 SAR images in pollution monitoring*. *Proc. IGARSS'94*, *vol. 4* (pp. 1954–1956).

Wahl, T., Skøelv, Å., Pedersen, J. P., Seljelv, L. -G., Andersen, J. H., Follum, O. A., et al. (1996). Radar satellites: A new tool for pollution monitoring in coastal waters. *Coastal Management*, *24*, 61–71.

Wu, S. Y., & Liu, A. K. (2003). Towards an automated ocean feature detection, extraction and classification scheme for SAR imagery. *International Journal of Remote Sensing*, *24*(5), 935–951.

Zhifu, S., Kai, Z., Baojiang, L., & Futao, L. (2002). Oil-spill monitoring using microwave radiometer. *Proc. IGARSS'02*, *vol. 5* (pp. 2980–2982).